Volume 69, Issue 3, 2025
Journal of Scientific Research
of
The Banaras Hindu University

Vibrational Resonance in a Parametric Quintic Oscillator with a Tunable Triple-Well Potential

M. Anisha Nashrin[1], Kairon Mubina M.S.[2], A. Ferin Fathima[3] and V. Chinnathambi[*,4]

[1]Department of Physics, Sadakathullah Appa College, Tirunelveli-627 011, Tamilnadu, India, Email: anishanashrin@gmail.com
[2]Department of Physics, Sadakathullah Appa College, Tirunelveli-627 011, Tamilnadu, India, Email: kaironmubinams@gmail.com
[3]Department of Physics, Sadakathullah Appa College, Tirunelveli-627 011, Tamilnadu, India, Email: ferin.fathima8@gmail.com
[*,4]Department of Physics, Sadakathullah Appa College, Tirunelveli-627 011, Tamilnadu, India, Email: veerchinnathambi@gmail.com
(Affiliated to Manonmaniam Sundaranar University, Tirunelveli 627 011, Tamilnadu, India)

***Abstract*—This study explores how the depth and location of a triple-well potential influence vibrational resonance in a parametric quintic oscillator driven by low- and high-frequency forces. Using the method of averaging, we derive the slow-motion equation and theoretical response amplitude, revealing that potential-well modifications strongly affect resonance behavior. System parameters (ω, Ω, d, q) are shown to modulate or suppress resonance peaks, offering control over vibrational responses. Bifurcation diagrams, resonance plot , and numerical simulations further confirm the theoretical results.**

***Index Terms*—Parametric quintic oscillator, Triple-well potential, Vibrational resonance, Chaos.**

I. Introduction

Parametrically excited systems, studied since Faraday's seminal work and Mathieu's equation, continue to be of great interest due to phenomena like parametric resonance (Faraday, 1831; Mathieu, 1838; Cartmel, 1990). These nonlinear oscillators model a wide array of scientific and engineering applications (Tchoukuegno, et al.; Adeyemi et al., 2023; Jia et al., 2016; Sahoo et al., 2021; Chen et al., 2021).

A particularly intriguing phenomenon in such systems is vibrational resonance (VR), where the synergistic effect of low- and high-frequency signals enhances the system's response (Landa et al., 2000; Gittermann, 2001). VR has been extensively investigated in various contexts, including monostable (Jeyakumari1 et al., 2009; Guo, 2011), bistable (Baltanas, 2003; Jeyakumari2 et al., 2009) and multistable systems (Rajasekar et al., 2011), as well as in excitable (Ullner et al., 2003), and time-delayed systems (Jeevarathinam, 2013). Significant recent interest has focused on systems subject to both parametric excitation and dual-frequency forces (Rajasekar et al., 2016; Roy et al., 2020, 2022). Notably, Nashrin et al. recently explored VR in parametrically driven quintic oscillators with multi-well potentials (AnishaNashrin et al., 2023, 2024). Building on previous work that analyzed VR in a damped, driven quintic oscillator with a triple-well potential, this paper investigates how variations in the depth and location of the wells influence VR in a parametrically excited triple-well system.

II. The Model

The linearly damped parametric quintic oscillator subjected to two periodic forces can be described as follows:

$$\ddot{x} + d\dot{x} + A\omega_0^2(1 + q\cos\omega_p t)x + B\beta x^3 + C\gamma x^5 = f\cos\omega t + g\cos\Omega t, \quad (1)$$

where $\Omega \gg \omega$ and the potential of the system is given by

$$V(x) = \frac{1}{2}A\omega_0^2(1 + q\cos\omega_p t)x^2 + \frac{1}{4}B\beta x^4 + \frac{1}{6}C\gamma x^6. \quad (2)$$

In Eq. (1), d represents the damping coefficient, where the term $f\cos\omega t$ denotes the lower frequency drive and $g\cos\Omega t$ represents the high-frequency drive. Parametric excitation is introduced through the term $q\cos\omega_p t$, where q stands for the amplitude of the parametric excitation and the parametric frequency is set to $\omega = \omega_p$. For $\omega_0^2, \gamma, A, B, C > 0$, $\beta < 0$ with $\beta^2 > 4\omega_0^2\gamma$, the potential $V(x)$ takes on a symmetric triple-well form. It's notable that the function $(1 + q\cos\omega_p t)$ is always positive when the parameter q falls within the range $-1 < q < 1$. This condition ensures that the shape of the potential consistently retains a triple-well form. If the parameters $\omega_0^2 = 3$, $\beta = -4$, $\gamma = 1$ are fixed, system factors A, B, C are considered. When $A = B = C = \alpha_1$, potential has a three minima at $x_1^* = 0$, $x_{2,3}^* = \pm\sqrt{\dfrac{-\beta + \sqrt{\beta^2 - 4\gamma\omega_0^2}}{2\gamma}}$ and two maxima at $x_{4,5}^* = \pm\sqrt{\dfrac{-\beta - \sqrt{\beta^2 - 4\gamma\omega_0^2}}{2\gamma}}$. The depths of the left- and right-wells denoted by $D_{\rm L}$ and $D_{\rm R}$ respectively are same and equal to $\alpha_1[6\omega_0^2 p + 3\beta p^2 + 2\gamma p^3]/12$, where

DOI: 10.37398/JSR.2025.690304

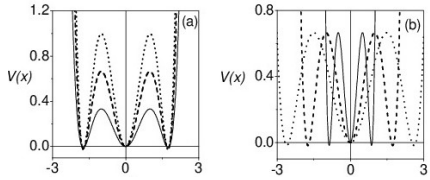

Fig. 1. Shape of the potential $V(x)$ for $\omega_0^2 = 3.0, \beta = -4.0, \gamma = 1.0$ and (a) $A = B = C = \alpha_1$ and (b) $A = \frac{1}{\alpha_2^2}, B = \frac{1}{\alpha_2^4}, C = \frac{1}{\alpha_2^6}$. In the subplots, the values of α_1 and α_2 for continuous line, dashed line and painted circles are 0.5, 1.0 and 1.5, respectively.

$p = \dfrac{-\beta - \sqrt{\beta^2 - 4\gamma\omega_0^2}}{2\gamma}$. By varying the parameter α_1 the depths of the two wells can be varied keeping the values of x_1^* and $x_{2,3}^*$ are kept constant. The system with $A = \dfrac{1}{\alpha_2^2}$, $B = \dfrac{1}{\alpha_2^4}$ and $C = \dfrac{1}{\alpha_2^6}$ with $\alpha_2 \neq 0$, the minima of $V(x)$ are $x_1^* = 0$, $x_{2,3}^* = \pm\alpha_2\sqrt{\dfrac{-\beta + \sqrt{\beta^2 - 4\gamma\omega_0^2}}{2\gamma}}$ and the maxima are $x_{4,5}^* = \pm\alpha_2\sqrt{\dfrac{-\beta - \sqrt{\beta^2 - 4\gamma\omega_0^2}}{2\gamma}}$ and in this case, $D_{\rm L} = D_{\rm R} = [6\omega_0^2 p + 3\beta p^2 + 2\gamma p^3]/12$ is independent of α_2. Thus, by varying α_2 the depth of the wells of $V(x)$ can be kept constant while the distance between the local maximum and the minima can be changed. Figures (1(a)) and (1(b)) illustrate the effect of α_1 and α_2. For convenience, the system (1) with $A = B = C = \alpha_1$ and $A = \frac{1}{\alpha_2^2}, B = \frac{1}{\alpha_2^4}, C = \frac{1}{\alpha_2^6}$ are represented by PS1 and PS2 respectively. Building on previous studies of how well depth and location affect vibrational resonance (VR) in multi-well systems (Rajasekar et al., 2010; Arathi et al., 2013; Ravisankar et al., 2012; Chen et al., 2018), this work analyzes these effects in a parametrically excited triple-well system. Specifically, we investigate how the depth of the wells and the distance between a minimum and a local maximum of the potential influence the occurrence of VR for arbitrary system parameters α_1 and α_2.

III. Theoretical Analysis of VR

First, we derive an expression for the effective frequency and effective potential using the parametric and fast frequency drives. Then, we establish a functional relation between the response amplitude $a_0(\omega)$ and the amplitude of the high-frequency drive g.

A. Effective frequency

For $\Omega \gg \omega$, owing to the disparity in time scales between the low-frequency force $f\cos\omega t$ and the high-frequency force $g\cos\Omega t$, it is reasonable to assume that the solution of the system (Eq.1) consists of a slow motion $s(t)$ with a period of $2\pi/\omega$ and a fast motion $\psi(t, \Omega t)$ with a period of $2\pi/\Omega$ (or a period of 2π in the fast time $\tau = \Omega t$), i.e., $x = s(t) + \psi(t, \tau)$. The mean value with respect to the fast time τ is given by

$$< \psi(t,\tau) >= \frac{1}{2\pi}\int_0^{2\pi} \psi(t,\tau)d\tau = 0. \tag{3}$$

Now substituting the solution $x = s + \psi$ in Eq.(1), we get

$$\begin{aligned} \ddot{s} + \ddot{\psi} + d\dot{s} + d\dot{\psi} + A\omega_0^2(1 + q\cos\omega_p t)s + \\ A\omega_0^2(1 + q\cos\omega_p t)\psi + \\ B\beta(s^3 + 3s^2\psi + 3s\psi^2 + \psi^3) + \\ C\gamma(s^5 + 5s^4\psi + 5s\psi^4 + 10s^3\psi^2 + 10s^2\psi^3 + \psi^5) \\ = f\cos\omega t + g\cos\Omega t. \end{aligned} \tag{4}$$

Using Eq.(3) and averaging the Eq.(4) with respect to fast time τ, we have

$$\begin{aligned} \ddot{s} + \ddot{\psi} + d\dot{s} + d\dot{\psi} + sF_0(t) + \psi F_0(t) \\ +B\beta\left(s^3 + 3s^2\psi + 3s\psi^2 + \psi^3\right) \\ +B\beta\left[(\psi^3 - <\psi^3>) + 3s^2(\psi - <\psi>) + 3s(\psi^2 - <\psi^2>)\right] \\ +C\gamma\left[s^5 + 5s^4\psi + 5s\psi^4 + 10s^3\psi^2 + 10s^2\psi^3 + \psi^5\right] \\ +C\gamma\left[(\psi^5 - <\psi^5> + 5s^4(\psi - <\psi>) + 5s(\psi^4 - <\psi^4>)\right] \\ +C\gamma\left[10s^3(\psi^2 - <\psi^2>) + 10s^2(\psi^3 - <\psi^3>)\right] = \\ f\cos\omega t + g\cos\omega t. \end{aligned} \tag{5}$$

Because ψ is a fast motion, we assume that $\ddot{\psi} \gg \dot{\psi}, \psi, \psi^2, \psi^3, \psi^4, \psi^5$. This allows us to split the Eq.(5) into the following equation of motion for s and ψ.

$$\ddot{s} + d\dot{s} + sF_0(t) + B\beta F_1(s,\psi) + C\gamma F_2(s,\psi) = f\cos\omega t. \tag{6}$$

$$\ddot{\psi} + d\dot{\psi} + \psi F_0(t) + B\beta F_3(s,\psi) + C\gamma F_4(s,\psi) = g\cos\Omega t, \tag{7}$$

where

$$\begin{aligned} F_0(t) &= A\omega_0^2(1 + q\cos\omega_p t) \\ F_1(s,\psi) &= s^3 + 3s^2 <\psi> + 3s <\psi^2> + <\psi^3> \\ F_2(s,\psi) &= s^5 + 5s^4 <\psi> + 5s <\psi^4> + 10s^3 <\psi^2> + \\ &\quad 10s^2 <\psi^3> + <\psi^5> \\ F_3(s,\psi) &= (\psi^3 - <\psi^3>) + 3s^2(\psi - <\psi>) + 3s(\psi^2 - <\psi^2>) \\ F_4(s,\psi) &= (\psi^5 - <\psi^5>) + 5s^4(\psi - <\psi>) + 5s(\psi^4 - <\psi^4>) \\ &\quad + 10s^3(\psi^2 - <\psi^2>) + 10s^2(\psi^3 - <\psi^3>) \end{aligned}$$

In Eq. (7), since the terms $B\beta F_3$ and $C\gamma F_4$ are smaller than the others, we ignore them and proceed to solve the rest of the equation self-consistently (by first disregarding the parametrically oscillating term, solving the remaining equation, and finally reintroducing this term) to obtain the equation

$$\ddot{\psi} + d\dot{\psi} = gU\cos(\Omega t + \phi) + gV\left[\cos(\chi t + \alpha) + \cos(\xi t + \alpha)\right], \tag{8}$$

where χ, ξ are new frequencies and U, V are new amplitude factors, which are defined as

$$\begin{aligned} \chi &= \Omega + \omega_p, \qquad \xi = \Omega - \omega_p \\ U &= [(\Omega^2 - A\omega_0^2)^2 + d^2\Omega^2]^{1/2}/\Omega(\Omega^2 + d^2)^{1/2} \\ V &= \frac{qR}{2}; \quad R = \frac{A\omega_0^2}{\Omega\sqrt{\Omega^2 + d^2}}. \end{aligned}$$

Also, the new phase terms are

$$\alpha = \tan^{-1}\left[\frac{d}{\Omega}\right], \quad \phi = \tan^{-1}\left[\frac{d\Omega}{\Omega^2 - A\omega_0^2}\right] \tag{9}$$

The solution of Eq.(8) evaluates with three forcing terms and is given by

$$\psi(t) = \frac{g}{\mu_1}\cos(\Omega t + \phi + \theta) + \frac{g}{\mu_2}\cos(\chi t + \alpha + \delta) + \frac{g}{\mu_3}\cos(\xi t + \alpha + \nu) \quad (10)$$

Substituting the first and second derivatives of $\psi(t)$ in Eq.(8) and equating the coefficients, we get the additional amplitudes and phase terms are

$$\begin{aligned}
\mu_1 &= \frac{\Omega^2(\Omega^2+d^2)}{\sqrt{(\Omega^2 - A\omega_0^2)^2 + \Omega^2 d^2}},\ \theta = \tan^{-1}(d/\Omega) \\
\mu_2 &= \frac{2\chi\Omega}{qA\omega_0^2}\left[(\chi^2+d^2)(\Omega^2+d^2)\right]^{1/2},\ \delta = \tan^{-1}(d/\chi) \\
\mu_3 &= \frac{2\xi\Omega}{qA\omega_0^2}\left[(\xi^2+d^2)\,(\Omega^2+d^2)\right]^{1/2},\ \nu = \tan^{-1}(d/\xi)
\end{aligned}$$

From Eq.(10), it follows that the averages of $\psi(t)$ are $<\psi>=<\psi^3>=<\psi^5>=0$, $<\psi^2(t)>=\frac{g^2}{2}\sum\frac{1}{\mu_i^2}$, and $<\psi^4(t)>=\frac{3}{8}g^4\sum\frac{1}{\mu_i^4}$, where $i=1,2,3$. The values of the averages of the $<\psi(t)>, <\psi^2>, <\psi^3>, <\psi^4>$ and $<\psi^5>$ can be invoked in Eq.(6) to obtain the following equation for the slow variable $s(t,\omega t)$ with the help of Eq.(8), which is

$$\ddot{s} + d\dot{s} + (\overline{\omega}^2 + A\omega_0^2 q\cos\omega_p t)s + \left[(B\beta + 10C\gamma <\psi^2>)s^3 + C\gamma s^5\right] = f\cos\omega t. \quad (11)$$

where

$$\begin{aligned}
\overline{\omega}^2(g) &= 3\beta' <\psi^2> + 5C\gamma <\psi^4> + A\omega_0^2 \\
&= \frac{3}{2}g^2\beta'\sum_{i=1}^{3}\frac{1}{\mu_i^2} + \frac{15}{8}C\gamma g^4\sum_{i=1}^{3}\frac{1}{\mu_i^4} + A\omega_0^2
\end{aligned} \quad (12)$$

where

$$\beta' = B\beta + 10C\gamma <\psi^2> = B\beta + 5C\gamma g^2\sum_{i=1}^{3}\frac{1}{\mu_i^2} \quad (13)$$

From Eq.(11), we defined the time dependent effective fequency as

$$\omega_{eff}(t) = \sqrt{\overline{\omega}^2 + A\omega_0^2 q\cos\omega_p t}, \quad (14)$$

and the effective potential is given by

$$V_{eff}(s,t) = \frac{1}{2}\omega_{eff}^2(t)s^2 + \frac{1}{4}\beta' s^4 + \frac{1}{6}C\gamma s^6 \quad (15)$$

From Eqs. (1) and (15), we observe a structural change in the system. In Eq. (11), the term $(\overline{\omega}^2 + A\omega_0^2 q\cos\omega_p t) > 0$, indicating that the effective equation describes a forced parametric quintic oscillator within an oscillatory potential affected by the high-frequency forcing $g\cos\Omega t$ term.

B. The flow equations

To proceed, we derive the amplitude and phase flow equations from Eq. (1), substituting the parametric frequency (ω_p) with the slow drive frequency (ω), i.e., $\omega = \omega_p$. The flow equations are obtained using standard perturbation techniques, such as the method of averaging. The primary objective of this study is to investigate the nonlinear response when the oscillator's natural frequency (ω_0) aligns with the low-frequency drive (ω), known as the primary resonance. This is achieved by finely tuning ω to be close to the frequency $\overline{\omega}$ specified in Eq. (12). To facilitate this exploration, we introduce a detuning parameter $\overline{\sigma}$, expressing ω as $\overline{\omega} + \epsilon\overline{\sigma}$, where ϵ serves as a perturbation parameter. To apply the perturbation technique, Eq. (11) is rearranged as follows:

$$\ddot{s} + \overline{\omega}^2 s = \epsilon\left[-d\dot{s} - A\omega_0^2 q(\cos\omega t)s - \beta' s^3 - C\gamma s^5 + f\cos\omega t\right] \quad (16)$$

Introducing the rescaled the parameters $\frac{\overline{\omega}^2}{\omega^2} = 1 - \epsilon\sigma, \Gamma = \frac{d}{\omega^2}, \Lambda = \frac{\beta'}{\omega^2}, \alpha = \frac{C\gamma}{\omega^2}, m = f/\omega^2$ and $K = \frac{A\omega_0}{\omega^2}$. Calculations become simpler on introducing a dimensionless time $\tau = \omega t$ and rewriting the Eq. (16) as

$$\ddot{s} + s = \epsilon\left[-\Gamma\dot{s} + K\cos\tau s + \Lambda s^3 + \alpha s^5 + f\cos\tau + \sigma s\right] \quad (17)$$

The flow equations can be derived through the method of averaging, the details of which have been described in refs. (Roy et al., 2020, 2022). By employing the method of averaging, we express $s = u\cos\omega t - v\sin\omega t$ with $u(t) = a(t)\cos\theta(t)$ and $v(t) = a(t)\sin\theta(t)$ and proceed as usual (Roy et al., 2020, 2022), arriving at the amplitude and phase flow equations.

$$\dot{a} = -\omega\left[\Gamma a + m\sin\theta\right], \quad (18)$$

and

$$\dot{\theta} = \omega\left[-\sigma + \frac{3}{4}\Lambda a^2 + \frac{5}{8}\alpha a^4 - \frac{m}{a}\cos\theta\right] \quad (19)$$

For the fixed points (a_0, θ_0) of this dynamical system, we obtain the following expression in the modified detuning parameter σ as,

$$\sigma = \left[\frac{3}{4}\Lambda a_0^2 + \frac{5}{8}\alpha a_0^4\right] \pm \sqrt{\frac{m^2}{a_0^2} - \Gamma^2} \quad (20)$$

Now substitute the Eq. (20) in the modified detuning parameter, then $\overline{\omega}^2 = \omega^2 - \epsilon\omega^2\sigma$, ie., $\frac{\overline{\omega}^2}{\omega^2} = 1 - \epsilon\sigma$,

$$\overline{\omega}^2 = \omega^2 - \epsilon\left\{\left[\frac{3\beta' a_0^2}{4} + \frac{5}{8}C\gamma a_0^4\right] \pm \sqrt{\frac{f^2}{a_0^2} - d^2\omega^2}\right\} \quad (21)$$

Substituting the value of β' in Eq. (13), we get

$$\overline{\omega}^2 = \frac{3}{2}g^2\beta\sum_{i=1}^{3}\frac{1}{\mu_i^2} + \frac{75}{8}\gamma g^4\sum_{i=1}^{3}\frac{1}{\mu_i^4} + A\omega_0^2 \quad (22)$$

Now combining the Eqs. (12) and (21), we get

$$\frac{3}{2}g^2\beta'\sum_{i=1}^{3}\frac{1}{\mu_i^2} + \frac{15}{8}C\gamma g^4\sum_{i=1}^{3}\frac{1}{\mu_i^4} = (\omega^2 - A\omega_0^2) - \epsilon\left\{\left[\frac{3\beta' a_0^2}{4} + \frac{5}{8}C\gamma a_0^4\right] \pm \sqrt{\frac{f^2}{a_0^2} - d^2\omega^2}\right\} \quad (23)$$

In Eq. (23), a functional relationship is established between the nonlinear response amplitude (a_0) and the strength of the high-frequency drive (g). This relationship reveals that the high-frequency forcing serves to amplify the resonant response to the low-frequency drive (ω). Subsequent sections delve into the influence of the depth and location of a triple-well potential on vibrational resonance in a parametrically driven quintic oscillator.

IV. Numerical Analysis

A. Vibrational Resonance through Potential Well Depth

Initially, we focus on system PS1, characterized by parameters $A = B = C = \alpha_1$. In this investigation, parameter values are fixed at $\omega_0^2 = 3.0$, $\beta = -4.0$, $\gamma = 1.0$, and $f = 0.05$. The theoretical response amplitude $a_0(\omega)$ of system PS1 is computed from Eq. (23). For numerical analysis of Eq. (1), we utilize the fourth-order Runge-Kutta scheme with time step sizes of $\Delta t = 0.001$. Initial conditions are set as $x(0) = 0.1$ and $y(0) = 0.1$, and the total simulation time is $t = 4000$, with the exclusion of the first 100 iterates to accommodate transients. To validate the theoretical predictions from Eq. (23), numerical results are obtained using the equations.

$$a_0(\omega) = \frac{\sqrt{a_0(\omega)_{\rm s}^2 + a_0(\omega)_{\rm c}^2}}{f}, \tag{24}$$

where

$$a_0(\omega)_{\rm s} = \frac{2}{nT}\int_0^{nT} x(t)\sin\omega t {\rm d}t,$$
$$a_0(\omega)_{\rm c} = \frac{2}{nT}\int_0^{nT} x(t)\cos\omega t {\rm d}t,$$

with $T = 2\pi/\omega$ and $n = 200$.

Initially, we investigate the effect of the depth of the wells (α_1) on vibrational resonance by varying the amplitude of the high-frequency force (g), both analytically and numerically. Figure 2 depicts the plot of $a_0(\omega)$ for four values of α_1 (= 0.25, 0.5, 1.0, 1.5), computed from Eq. (23) and superimposed with the corresponding numerical curves obtained from Eq. (24) using Eq. (1) for comparison. The continuous curves represent the theoretically calculated $a_0(\omega)$ from Eq. (23), while the painted circles represent numerically computed Q from Eq. (26). From Fig. 2, it is evident that, for $\alpha_1 < 1$, three peaks are observed with varying amplitudes. Conversely, for $\alpha_1 > 1$, four resonances are observed, all with higher amplitudes.

For example, when $\alpha_1 = 0.25$, three resonances occur: one with a higher amplitude at $g = 180.95$ with $a_0(\omega) = 0.665$, and the other two with smaller amplitudes at $g = (101.23, 149.04)$ with the response amplitudes $a_0(\omega) = (0.125, 0.131)$, as depicted in Fig. 2(a). For $\alpha_1 = 0.5$, all three resonances occur with higher amplitudes at different g values. Specifically, the three prominent peaks are observed at $g = (30.54, 90.18, 172.73)$ with the response amplitudes $a_0(\omega) = (0.674, 0.895, 0.667)$, as shown in Fig. 2(b). Similarly, for $\alpha_1 = 1.0$, four prominent peaks are observed at $g = (60.38, 85.15, 154.85, 165.86)$ with the response amplitudes $a_0(\omega) = (0.661, 0.927, 0.401, 0.629)$, and for $\alpha_1 = 1.5$, four prominent peaks are observed at

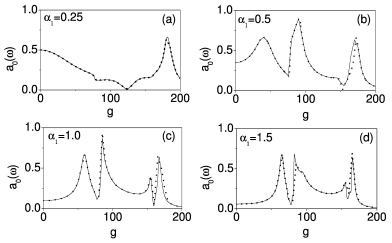

Fig. 2. Response amplitude $a_0(\omega)$ versus g for four values of α_1 with $\Omega = 10$. The theoretical and numerical values of $a_0(\omega)$ are represented by continuous lines and painted circles. The other parameters values are fixed at $\omega_0^2 = 3.0, \beta = -4.0, \gamma = 1.0, d = 0.3, q = 0.1, f = 0.05, \Omega = 10$ and $\omega = \omega_p = 1.0$.

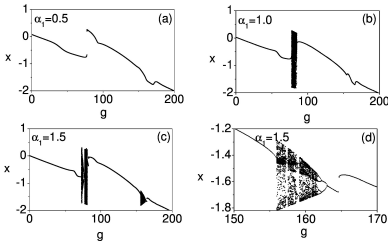

Fig. 3. Bifurcation diagrams of Eq.(1) for four values of α_1. The values of x are collected at $t = n \times (2\pi/\omega)$, $n = 1, 2, ..., 200$ after leaving suffient transient motion. The values of the parameters are $\omega_0^2 = 3.0, \beta = -4.0, \gamma = 1.0, d = 0.3, q = 0.1, f = 0.05, \Omega = 10$ and $\omega = \omega_p = 1.0$.

$g = (65.21, 83.84, 154.98, 165.14)$ with the response amplitudes $a_0(\omega) = (0.669, 0.669, 0.323, 0.687)$, clearly illustrated in Figs. 2(c) and 2(d). From Fig. 2, it is evident that as the depth of the well increases, the non-resonance interval widens and the width of the resonances decreases. Figure 3 shows the bifurcation diagrams of Eq. (1). The analysis is confined to the range $0 < g < 200$. For $\alpha_1 = 0.5$, the period-T is observed in the above range of g, as depicted in Fig. 3(a). When $\alpha_1 = 1.0$, chaotic motion is observed for $g \in [77.15, 80.12]$, as shown in Fig. 3(b). For $\alpha_1 = 1.5$, chaotic motion and other periodic orbits are observed, as illustrated in Fig. 3(c). The magnification of Fig. 3(c) is shown in Fig. 3(d). From Fig. 3(d), it is evident that reverse periodic orbits, window regions, and chaotic motion are present.

To investigate the effect of α_1 on vibrational resonance for two values of the frequency (ω) of the low-frequency force $f\cos\omega t$, we illustrate the dependence of the response amplitude $a_0(\omega)$ on g with $\Omega = 12$, $\omega = \omega_p = 1.0$ in Fig. 4(a), and with $\Omega = 12$, $\omega = \omega_p = 1.5$ in Fig. 4(b). In Fig. 4(a), double resonances are observed for all values of α_1 with $\Omega = 12$, $\omega = 1.0$, whereas four resonances occur for $\Omega = 10$ with $\omega = 1.0$ (Fig. 2). Thus, the number of resonances decreases as the frequency Ω of the high-frequency force increases. The response curves for $\Omega = 12$ and $\omega = 1.5$ are depicted in Fig. 4(b) for three values of $\alpha_1 = 0.5, 1.0, 1.5$. Here again double resonances are observed for $\alpha_1 = 0.5, 1.0$ and 1.5. As we increase the values of ω, the number of resonances decreases. Additionally, the peaks of the first resonance decrease, but the second resonance increases as we increase the value of ω.

The influence of the depth of the potential wells (α_1) on

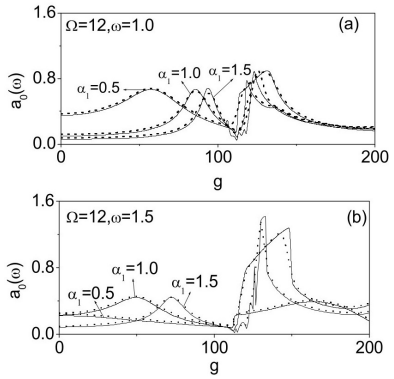

Fig. 4. Response amplitude $a_0(\omega)$ versus g for three values of α_1 with (a) $\Omega = 12, \omega = 1.0$ and (b) $\Omega = 12, \omega = 1.5$. The theoretical and numerical values of $a_0(\omega)$ are represented by continuous lines and painted circles. The other parameters values are fixed at $\omega_0^2 = 3.0, \beta = -4.0, \gamma = 1.0, d = 0.3, q = 0.1$ and $f = 0.05$.

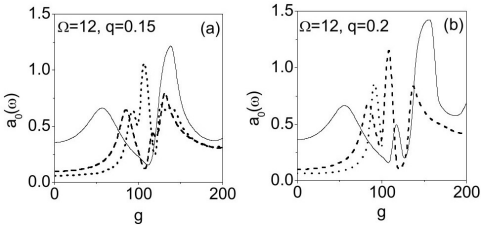

Fig. 5. The theoretical response amplitude $a_0(\omega)$ versus g for three values of α_1 with (a) $q = 0.15$ and (b) $q = 0.2$. Solid line corresponds to $\alpha_1 = 0.5$, dashed line for $\alpha_1 = 1.0$ and dotted line for $\alpha_1 = 1.5$. The values of the parameters are $\omega_0^2 = 3.0, \beta = -4.0, \gamma = 1.0, d = 0.3, \Omega = 12, f = 0.05$ and $\omega = \omega_p = 1.0$.

VR by varying the amplitude g of the high-frequency force for two values of the amplitude of the parametric excitation (q) is shown in Fig. 5. In Fig. 5, we have plotted the theoretical values of $a_0(\omega)$ against g for $\alpha_1 = 0.5, 1.0, 1.5$ with $q = 0.15$ and $q = 0.2$. The other parameter values are fixed at $\omega = \omega_p = 1.0$, $\Omega = 12$, and $d = 0.3$. The response curves for $q = 0.15$ are shown in Fig. 5(a). Triple resonances occur for $\alpha_1 = 1.0$ and 1.5, and two resonances occur for $\alpha_1 = 0.5$. The theoretical response curves for $q = 0.2$ are shown in Fig. 5(b). Here again, triple resonances occur for $\alpha_1 = 0.5$ and 1.0 within the range $0 < g < 200$. For $\alpha_1 = 1.5$, a single resonance occurs within the range $0 < g < 100.67$, and beyond this range, the motion is unbounded, as clearly shown in Fig.5(b). From Fig. 2 (For $q = 0.1$) and Fig.5 (For $q = 0.15, 0.2$), it is observed that as the amplitude of the parametric excitation q increases, the number of resonances decreases, but the resonance amplitude and width of the resonances increase. Next, we consider the effect of the depth of the potential wells (α_1) on VR by varying the amplitude g of the high-frequency force for two values of the damping strength d of the system. Figure 6 shows the theoretical response amplitude $a_0(\omega)$ as a function of g for three values of $\alpha_1 = 0.5, 1.0, 1.5$ with $d = 0.1$ and $d = 0.2$. From Fig. 6, the effect of damping strength d is clearly seen. When we increase the value of damping strength (d) from 0.1 to 0.2, we clearly observe that the maximum of the response amplitude decreases.

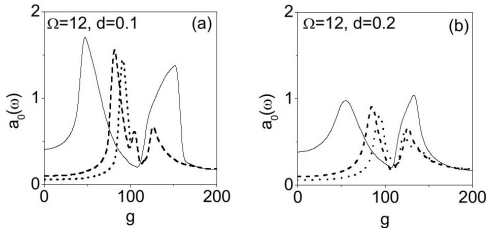

Fig. 6. The theoretical response amplitude $a_0(\omega)$ versus g for three values of α_1 with (a) $d = 0.1$ and (b) $d = 0.2$. Solid line corresponds to $\alpha_1 = 0.5$, dashed line for $\alpha_1 = 1.0$ and dotted line for $\alpha_1 = 1.5$. The values of the parameters are $\omega_0^2 = 3.0, \beta = -4.0, \gamma = 1.0, \Omega = 12, q = 0.1, f = 0.05$ and $\omega = \omega_p = 1.0$.

B. Vibrational Resonance through Potential Well Location

The PS2 system is characterized by $A = 1/\alpha_2^2$, $B = 1/\alpha_2^4$, and $C = 1/\alpha_2^6$. As α_2 increases, the location of the two maxima of $V(x)$ gradually shifts away from the origin in the opposite direction, and the distance between the neighboring potential wells also increases. We initiate our examination of the resonance phenomenon in the PS2 system by considering the role of the location of maxima of the potential (α_2), as presented in Fig. 7. Fig.7 depicts the superimposed response curves illustrating the dependence of the response amplitude $a_0(\omega)$ on the amplitude g of the high-frequency signal for four values of $\alpha_2 = (0.5, 0.75, 1.0, 2.0)$ with $\Omega = 10$. The continuous lines represent the response curves of theoretically computed $a_0(\omega)$ values, while the painted circles represent corresponding numerical values. The other parameter values are $\omega_0^2 = 3.0$, $\omega = \omega_p = 1.0$, $\beta = -4.0$, $\gamma = 1.0$, $d = 0.3$, $q = 0.1$, and $f = 0.05$. For $\alpha_2 = 0.5$, one resonance peak is observed with a higher response amplitude $a_0(\omega)$ at $g = 10.512$, and two other resonances occur with smaller amplitude at $g = 14.627$ and $g = 17.175$ within the range $0 < g < 20$. Beyond this range, i.e., $g > 20$, the motion is unbounded for $\alpha_2 = 0.5$, as clearly seen in Fig.7(a). The response curves for $\alpha_2 = 0.75$ are shown in Fig.7(b). Single resonance is observed at $g = 32.876$ within the range $0 < g < 40$. Beyond this range, i.e., $g > 40$, the motion is unbounded. From Fig.7, for $\alpha_2 < 1$, resonances are observed within a narrow range g, beyond which unbounded motion occurs. For $\alpha_2 = 1.0$, the PS2 system shows four resonance peaks, whereas double resonances occur for $\alpha_2 = 1.5$ within the interval $0 < g < 200$. This is clearly evident in Figs.7(c) and 7(d). By comparison with the PS1 system, the non-resonance intervals increase in the PS2 system compared to the PS1 system (Figs. 2 and 7).

Next, we investigate the effect of α_2 on vibrational resonance (VR) by varying the strength of the parametric excitation (q) in the PS2 system. The results are presented in Fig. 8(a). For $q = 0.1$ and $q = 0.3$, double resonances occur with smaller response amplitude, whereas single resonance is observed for $q = 0.5$ with a larger response amplitude, which is clearly seen in Fig. 8(a). From Fig. 8(a), we observe that as q increases, the response amplitude also increases, but the number of resonances decreases. By making the comparison

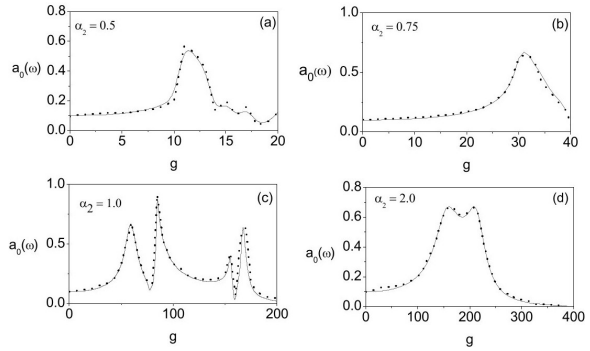

Fig. 7. Response amplitude $a_0(\omega)$ versus g for four values of α_2 with $\Omega = 10$. The theoretical and numerical values of $a_0(\omega)$ are represented by continuous lines and painted circles. The other parameters values are fixed at $\omega_0^2 = 3.0, \beta = -4.0, \gamma = 1.0, d = 0.3, q = 0.1, f = 0.05, \Omega = 10$ and $\omega = \omega_p = 1.0$.

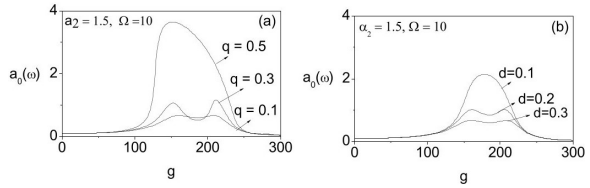

Fig. 8. (a) The theoretical response amplitude $a_0(\omega)$ versus g for three values of q with $\alpha_2 = 1.5, d = 0.3$ and $\Omega = 10$. (b) The response amplitude $a_0(\omega)$ versus g for three values of d with $\alpha_2 = 1.5, q = 0.1$ and $\Omega = 10$. The values of the parameters are $\omega_0^2 = 3.0, \beta = -4.0, \gamma = 1.0, f = 0.05$ and $\omega = \omega_p = 1.0$.

with the PS1 system, as the values of q increase, the number of resonances decreases but the maximum of the response amplitude increases. The effect of damping strength d is illustrated in Fig. 8(b). Figure 8(b) presents the evolution of the response amplitude $a_0(\omega)$ versus g for three values of d with $\alpha_2 = 1.5$, $q = 0.1$, and $\Omega = 10$. In Fig. 8(b), for $d = 0.1$, single resonance occurs, whereas double resonances occur for $d = 0.2$ and $d = 0.3$. It is clearly observed that as d increases, the maximum of the response amplitude $a_0(\omega)$ decreases, but the number of resonances increases.

V. Conclusion

This study analyzed how well depth and location control vibrational resonance (VR) in a parametrically excited triple-well oscillator. Using analytical methods, we derived the system's response amplitude and showed how parameters α_1 and α_2 regulate the number and position of resonances. Additional parameters (Ω, q, ω, d) further enable precise suppression or induction of resonance. Bifurcation and resonance analyses revealed that the system can exhibit up to four resonances, with distinct bounded and unbounded behaviors in PS1 and PS2 systems. Future work should extend this analysis to asymmetric double-well and nonlinearly damped systems.

References

Adeyemi C., Kpomahou Y.J.F., Agbelele J.K., Adechinan A.J., & Yamadjako A.F., (2023) Effects of periodic parametric damping and amplitude-modulated signal on vibrational resonance and torus-doubling bifurcations occurrence in an asymmetric mixed Rayleigh-Liénard oscillator, *Phys. Scr.*, 98, 105204, . DOI 10.1088/1402-4896/acf3ad

Anisha Nashrin M., Abdul kader S.M., Sethu Meenakshi M.V., Chinnathambi V., & Rajasekar S., (2023) Analysis of vibrational resonance in a parametric quintic oscillator with double-well potentials, *Dynamic Systems and Applications*, 32, 294-313.

Anisha Nashrin M., Abdul kader S.M., Zeenath Bazeera A., Chinnathambi V., & Rajasekar S., (2024) Impact of Parametric Excitation on vibrational resonance in a Symmetric Triple-well system, *Nonlinear Studies*, 31(1), 309-325.

Arathi S., & Rajasekar S., (2011) Impact of the depth of the wells and multifractal analysis on stochastic resonance in a triple-well system, *Phys. Scr.*, 84, 065011(7pp), doi.10.1088/0031-8949/84/06/065101.

Baltanas J.B., Lopez L., Blechman I.I., Landa P.S., Zaikin A., & Kurths J., (2003) Experimental Evidence, Numerics, and Theory of Vibrational Resonance in Bistable Systems, *Phys. Rev. E*, 67, 066119. DOI:https://doi.org/10.1103/PhysRevE.67.066119

Cartmell M., (1990) *Introduction to Linear, Parametric and Nonlinear vibrations*, Chapman and Hall, London.

Chen K., He S., Song Y., Wu L., Wang K., & Zhang M., (2021) The Numerical Analysis for Parametric Resonance of Multicable System considering Interaction between Adjacent Beam Portions, Hindawi, *Shock and Vibration*, Volume 2021, Article ID 6937794, 19 pages, https://doi.org/10.1155/2021/6937794

Chen Z., & Ning L., (2018) Impact of depth and location of the wells on vibarional resonance in a triple-well system, *Pramana-J. Phys.*, 90, 49-58. https://doi.org/10.1007/s12043-018-1539-8.

Faraday M., (1831) Xvii. On a Peculiar Class of Acoustical Figures; and on Certain Forms Assumed by Groups of Particles upon Vibrating Elastic Surfaces., *Phil. Trans. R. Soc. London*, 121, 299.

Gittermann M., (2001), Bistable oscillator driven by two periodic fields, *J. Phys. A: Math. Gen.,* 34, L355-L357. DOI: https://doi.org/10.1088/0305-4470/34/24/101

Guo F., (2011) Multiplicative noise-induced vibrational resonance in a monostable system with one high-frequency and two low-frequency forces, *Physica Scripta*, 83(2), 025008. doi:10.1088/0031-8949/83/02/025008.

Jeevarathinam C., Rajasekar S., & Sanjuan M.A.F, (2013) Effect of multiple time-delay on vibrational resonance, Chaos, 23(1), 013136.

Jeyakumari S, Chinnathambi V., Rajasekar S. & Sanjuan M.A.F., (2009) Single and multiple vibrational resonance in a quintic oscillator with monostable potentials, *Phys. Rev.E*, 80, 046608.

Jeyakumari S, Chinnathambi V, Rajasekar S & Sanjuan M.A.F., (2009) Analysis of vibrational resonance in a quintic oscillator, *Chaos*, 19, 043128-8.

Jia Yu., Sijun Du, Ashwin & Seshia A., (2016) Twenty-Eight Orders of Parametric Resonance in a Microelectromechanical Device for Multi-band Vibration Energy Harvesting, *Scientific Reports*, 6(1), 30167.

Landa P.S., & McClintock P.V.E., (2000) Vibrational resonance, *J. Phys.A: Math. Gen.,* 33, L433-L438. DOI https://doi.org/10.1088/0305-4470/33/45/103

Mathieu E, (1868) Memoire sur Le Mouvement Vibratoire d'une Membrane de forme Elliptique, *J. Math. Pures Appl.*, 13, 137-203.

Rajasekar S., Abirami K., & Sanjuan M.A.F., (2011) Novel Vibrational Resonance in Multistable Systems, *Chaos*, 21, 033106. https://doi.org/10.1063/1.3610213

Rajasekar S., & Sanjuán M.A.F., *Nonlinear Resonances*, Springer Series in Synergetics, Springer, Switzerland, 2016

Rajasekar S., Jeyakumari S., Chinnathambi V., & Sanjuan M.A.F., (2010) Role of depth and location of minima of a double-well potential on vibrational resonance, *J.Phys.A:Math.Theor.*, 43, 465101(11pp). doi:10.1088/1751-8113/43/46/465101.

Ravisankar L., Guruparan S., Jeyakumari S., & Chinnathambi V., (2012) Effect of depth and location of a double-well potential on vibrational resonance in a quintic oscillator, (*The Int. J. Eng. and Sci., 1(2), 81-92.*

Roy S.,, Das D., & Banerjee D., (2020) Nonlinear response of a parametric bistable oscillator with multiple excitation, Eur. Phys. J. B*, 93, 1-12.*

Roy S., Das D., & Banerjee D., (2022) Hopf bifurcation in vibrational resonance through modulation of fast frequency, arXiv. 2205.08091v1 [nlinCD] 17 May 2022.

Sahoo P.K., & Chatterjee S., (2021) High-frequency Vibrational Control of Principal Parametric Resonance of a Nonlinear Cantilever Beam: Theory and Experiment, Journal of Sound and Vibration*, 505, 116138.*

Tchoukuegno R & Woafo P, (2002) Dynamics and active control of a particle in a Φ^6*- potential with a parameter forcing,* Physica D*, 167, 86-100.*

Ullner E., Zaikin A., Garcia-Ojalvo J., Bascons R., & Kurths J., (2003) Vibrational resonance and Vibrational propagation in excitable system, Phys.Lett. A*, 312, 348-354. https://doi.org/10.1063/1.3076396*